Materials Research. 2018; 21(4): e20170729
DOI: http://dx.doi.org/10.1590/1980-5373-MR-2017-0729

Identification of Humidity Sensing Mechanism in $MgAl_2O_4$ by Impedance Spectroscopy as Function of Relative Humidity

Guilherme Baltar Crochemore[a], Amadeu Rodrigues Pereira Ito[a], Celso Antonio Goulart[a], Dulcina Pinatti Ferreira de Souza[a]*

[a]Departamento de Engenharia de Materiais, Universidade Federal de São Carlos, Rodovia Washington Luis, km 235, PO box 676, 13565-905, São Carlos, SP, Brasil

Received: August 10, 2017; Revised: February 20, 2018; Accepted: March 08, 2018

$MgAl_2O_4$ is a humidity sensing material, which high melting point requires high sintering temperatures. In this work, manganese oxide was used as a sintering aid to obtain $MgAl_2O_4$ samples sintered at 1350°C with a microstructure suitable for humidity sensing. Impedance spectroscopy analyses were performed at several levels of relative humidity, indicating that this correlation is possible within the range of 10-80% of relative humidity.

Keywords: *$MgAl_2O_4$, humidity sensors, impedance spectroscopy.*

1. Introduction

The need for measured and controlled humidity in a variety of environments has led to intense research of materials which electrical properties change according to atmospheric humidity [1-3]. Many materials are classified as humidity sensors. These materials include porous ceramic oxides [1], which electrical characteristics vary according to relative humidity due to the ionic conduction produced by the adsorption and condensation of water molecules. The electrical conduction mechanisms responsible for humidity sensitivity in a wide range of relative humidity levels are described extensively in the literature for several porous ceramic oxides, including $MgAl_2O_4$ which has been reported in the literature since the 1980s [1,4-10].

The electrical conduction of humidity sensitive porous ceramic oxides as a function of relative humidity can be described as follows: chemical adsorption of water molecules occurs at low humidity. After the first layer of chemically adsorbed molecules is formed, dissociation occurs, resulting in hydroxyl ions (OH^-) and protons (H^+). The conduction of protons in the chemically adsorbed water monolayer occurs through the hopping mechanism. With increased humidity, layers of water molecules are adsorbed physically onto the chemically adsorbed layer, binding to the hydroxyl group (OH^-) and generating H_3O^+, which then becomes the dominant charge carrier. The migration of protons occurs according to the chain exchange reaction $H_3O^+ + H_2O = H_2O + H_3O^+$. As humidity continues to increase, a continuous film of water molecules is formed and the physically adsorbed water molecules are similar to liquid water. In this stage, the H^+ transfer takes place between adjacent water molecules and the electrical conduction mechanism is the so-called Grotthuss chain reaction ($2H_2O = H_3O^+ + H^+$)[2,11].

In addition to the above described mechanisms, condensation of water vapor can start even at low humidity if there are pores with suitable sizes. The ratio of critical pore size to atmospheric humidity at which water condensation occurs is established by Kelvin's equation[1]. According to this equation, condensation of water vapor begins at room temperature in pores of 20 Å at a relative humidity of ~ 15% and continues up to ~ 1000 Å, at which point the atmosphere is water-saturated[12].

The main characteristics of humidity sensors are sensitivity, reproducibility and response time. In the case of porous ceramic humidity sensors, the microstructure developed during the sintering process, specifically the total porosity and pore size distribution, is responsible for these characteristics [1,13,14]. Microstructures with specific characteristics can be obtained by adding dopants that control the sintering mechanisms [15-17].

Many studies in the literature have used impedance spectroscopy to analyze the electrical response of humidity sensing materials[5-8,18]. However, the majority of spectra are highly complex, showing no predominant conduction mechanism attributable to specific microstructures.

In this work, Mn-doped $MgAl_2O_4$ samples were prepared by solid state reaction. Sintered samples were characterized by impedance spectroscopy at room temperature, aiming to link their electrical response to the predominant mechanism at several levels of relative humidity. The use of Mn as a sintering additive allowed the development of specific microstructures with relatively simple impedance spectra, enabling the identification of the predominant electrical conduction mechanisms in the range of 10 to 80% of relative humidity.

*e-mail: dulcina@ufscar.br

2. Experimental

2.1. Sample preparation

Mn-doped $MgAl_2O_4$ samples were prepared by solid state reaction, using aluminum oxide (Baikowsky CR-30), magnesium oxide (Synth) and manganese nitrate (Aldrich). Suitable amounts of each raw material were mixed in isopropanol alcohol with 2 wt% of polyvinyl butyral (B-98 Solutia) in a vibratory mill. Table 1 lists their compositions and respective identifications.

Table 1. Samples' identification

Sample identification	MgAl2O4 (mol %)	MnO additive (mol%)
A	100	-
B	98	2
C	96	4

The suspensions were dried at room temperature, after which the resulting powders were calcined at 600ºC in air for 1 hour. Calcined powders were deagglomerated through an 80 mesh nylon sieve. Pellets (13 mm diameter and 2 mm thickness) and plates (70 x 20 x 2 mm) of each composition were prepared by uniaxial pressing followed by isostatic pressing at 200 MPa. Five samples of each composition were sintered at different temperatures (1200-1600°C) for 2h in air in order to evaluate the evolution of porosity in function of temperature. The density and porosity of the sintered samples were measured using Archimedes' principle.

2.2. Sample characterization

The bulk densities and apparent porosity of the sintered samples were determined by the Archimedes' principle, using an analytical balance (Metler Toledo AX 204). X-ray diffraction was carried on sintered samples at room temperature (CuK_α, 2θ=15-80 º, 0.33 º/s) using a Siemens D5000 diffractometer, and cell parameters were determined by Rietveld refinement using the PANalytical X'Pert HighScore Plus software and ICSD (Inorganic Crystal Structure Database) CIF files. The pore size distribution was analyzed by Hg intrusion porosimetry (Micromeritics Porosizer 9320). The microstructure of fractured surfaces of sintered samples was analyzed by Scanning Electron Microscopy (SEM) (Phillips XL 30 FEG). Grain size and grain size distribution for each composition were analyzed using the SEM images with the software ImageJ and then treating the data with the software Minitab®. The pellets were characterized electrically by impedance spectroscopy (Impedance analyzer HP 4192A LF) in the frequency range of 5 Hz-13 MHz and an excitation voltage of 500 mV. Symmetrical Ag electrodes were applied on both surfaces of the pellets, which were then fired at 700°C. The impedance measurements were performed at room temperature with relative humidity varying from 10 to 80% during the water adsorption step. The relative humidity (r.h.) of the air was measured with a polymeric humidity sensor (Vaisala HMME 213).

To help interpret the impedance spectroscopy of the samples, distilled water was measured at room temperature in the same frequency range as that used for the samples with aluminum electrodes. Similar measurements were also taken of $MgAl_2O_4$ powder suspension filtration water. The experimental setup used for these measurements was similar to that used by Miranda et al. [19], as shown in Figure 1.

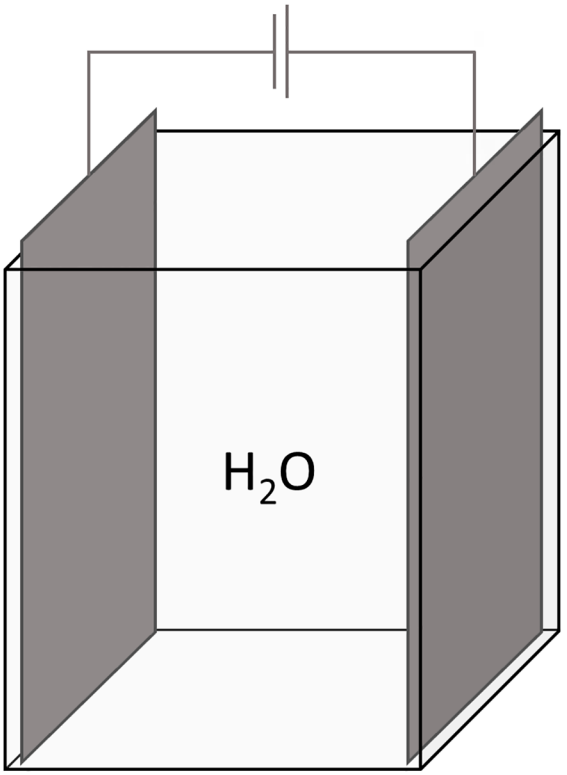

Figure 1. Scheme of the experimental setup used in impedance spectroscopy analysis of water

The samples' humidity sensing reproducibility and response time were determined based on four-probe dc measurements (HP 3458A multimeter) with Ag electrodes. The dc measurements were taken at room temperature and in both adsorption and desorption steps in the range of 10-80% of r.h.

3. Results and Discussion

3.1 Density, porosity, crystalline phases and microstructure

Figure 2 presents the evolution of relative density and apparent porosity in function of sintering temperature. The standard deviation for density and porosity mean

values was less than ± 0.001. Samples still show high porosity (≥ 50%) up to 1350°C, and above 1450°C porosity starts to drop, reaching values lower than 5% at 1600°C. Therefore, the temperature of 1350°C, which yielded open porosity around 50%, was selected for sintering, considering the desirable characteristics of humidity sensors. Table 2 summarizes the results of each composition sintered at 1350°C.

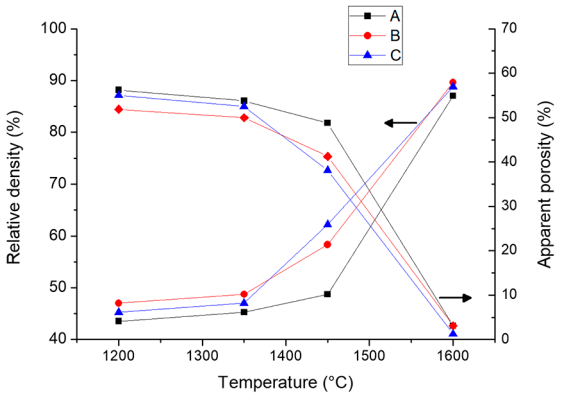

Figure 2. Relative density and apparent porosity in function of sintering temperature

Table 2. Relative density and total open porosity of samples sintered at 1350°C

Sample identification	Relative density (%)	Total open porosity (%)
A	45.0	54
B	49.0	50
C	46.7	53

Theoretical density of $MgAl_2O_4$ = 3.578 g/cm3

Figure 3 shows the pore size distributions determined by Hg intrusion porosimetry. Average pore diameter increased in response to the addition of Mn, showing 0.13, 0.26 and 0.39 µm for compositions A, B and C, respectively. However, the percentage of open pores and the relative density did not vary significantly (Figure 2 and Table 2). Samples having a similar total number of open pores and different average pore diameters are important for the evaluation of their electrical behavior at different levels of humidity.

Figure 4 depicts the microstructures of fracture surfaces analyzed by scanning electron microscopy and Figure 5 presents the grain size distribution data for each composition. The addition of manganese inhibited grain growth, maintaining the high specific surface area in compositions B and C, which is an important characteristic of ceramics used as humidity sensors.

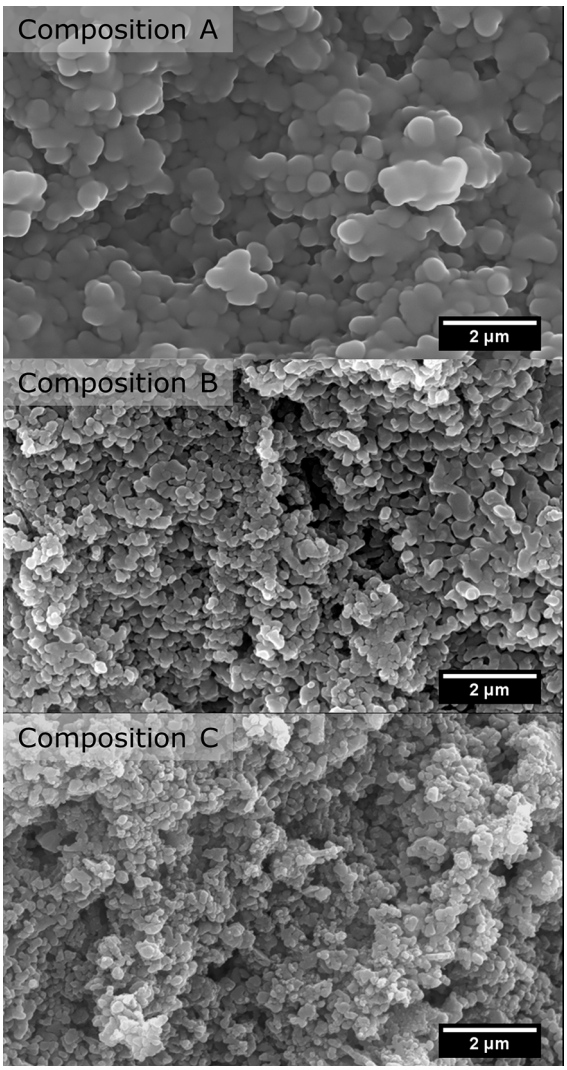

Figure 4. SEM micrographs of fracture surfaces from samples sintered at 1350°C

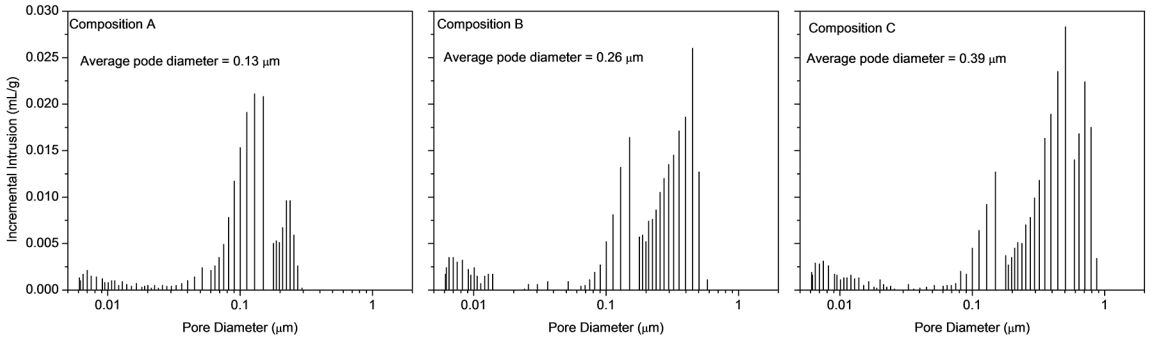

Figure 3. Pore size distributions obtained by Hg intrusion porosimetry

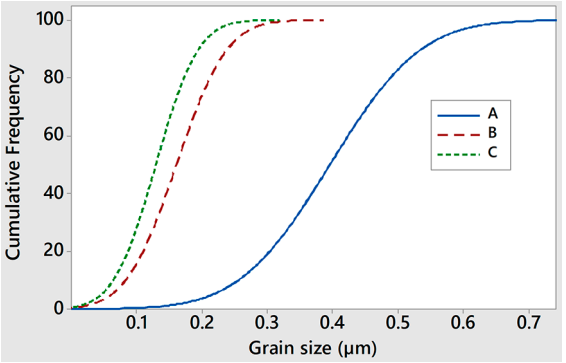

Figure 5. Grain size distribution for each composition sintered at1350°C

Figure 6 shows the X-ray diffraction patterns of pellets sintered at 1350°C and the cell parameters calculated by Rietveld refinement. All samples presented only $MgAl_2O_4$ cubic structure as crystalline phase, according to JCPDS card no. 21-1152 (Magnesium Aluminum Oxide, Spinel). Cell parameters increased in function of the dopant content, which may be attributed to the substitution of Mg^{2+} by Mn^{2+} ions in the A site of the spinel structure [20,21]. Mg^{2+} ions in tetrahedral coordination have an ionic radii of 0,57 Å, while Mn^{2+} ions have radii of 0,66 Å [22]. This process may be the reason behind the hindered grain growth presented by the Mn-doped samples.

3.2 Impedance spectra

Figures 7 and 8 illustrate the Nyquist plots resulting from these measurements. The fitting of the distilled water spectrum yielded a relaxation frequency (F_0) of 1.17 x 10^5 Hz and a decentralization angle (θ) of 0.8 deg. This low value for the decentralization angle, i.e., low relaxation time dispersion, indicates the presence of only one electrical conduction mechanism, the so-called Grotthuss chain reaction[11].

The spectrum of the water resulting from powder sedimentation, Figure 8, contains a semicircle with a low decentralization angle (0.90 deg) at a higher frequency (> 100 kHz). The fitting of this semicircle yielded a relaxation frequency of 1.60 x 10^6 Hz, which is one order of magnitude higher than that of the process obtained for distilled water (Figure 7). This process represents the electrolytic conduction of ions originating from the surface of $MgAl_2O_4$ particles. Figure 8 shows also a straight line

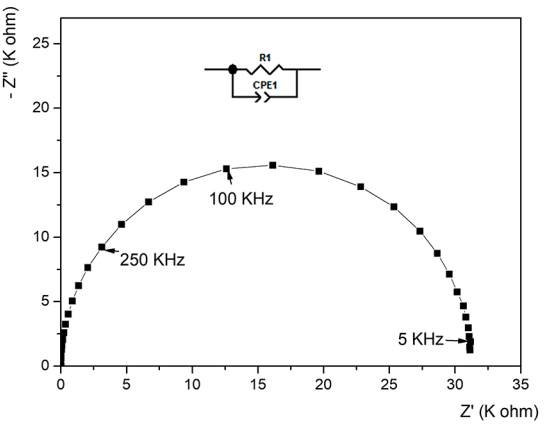

Figure 7. Equivalent circuit and Nyquist plot of distilled water at room temperature

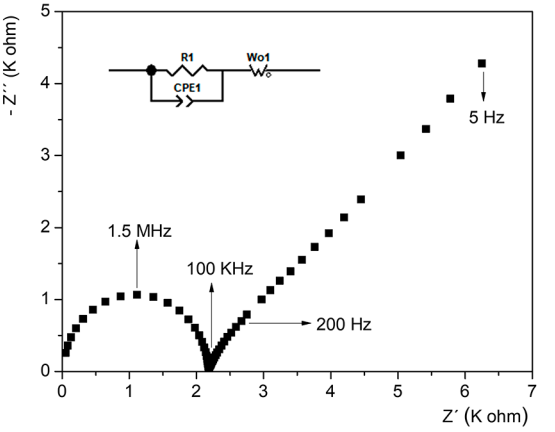

Figure 8. Equivalent circuit and Nyquist plot at room temperature of water resulting from $MgAl_2O_4$ powder suspension filtration

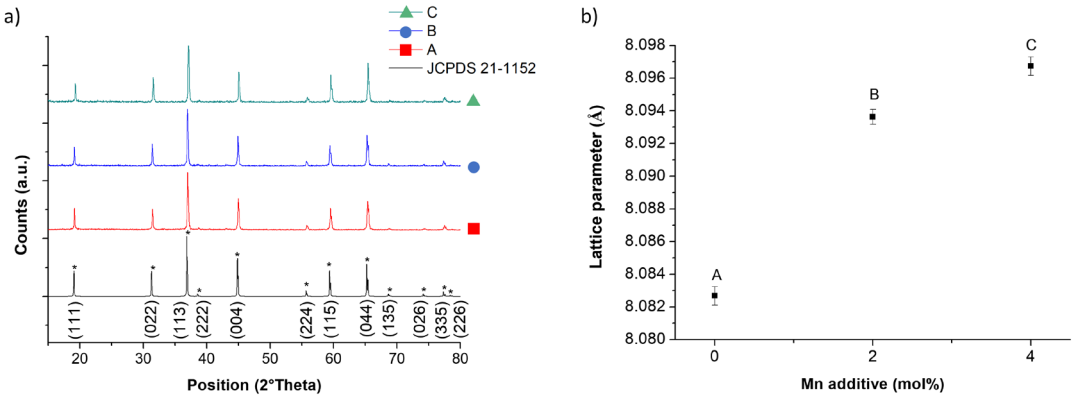

Figure 6. X-ray diffraction patterns of samples sintered at 1350°C (a) and the calculated cell parameters of each composition (b)

at frequencies lower than 100 KHz known as Warburg impedance which describes the ions diffusion through the electrode-electrolyte interface. Considering that this interface is not predominant in the samples, see Figures 9 to 11, this phenomenon will not be discussed in this article.

$MgAl_2O_4$ sintered pellets were analyzed by impedance spectroscopy at 25°C with relative humidity (r.h.) varying from 10 to 80%. Figures 9 to 11 show a sequence of spectra for compositions A, B and C, respectively.

At 4 and 12% r.h. the sample of composition A (Figure 9) remained highly resistive and behaved as a capacitor, especially at 4% r.h. At 25% r.h. the impedance spectrum presented a depressed semicircle with a decentralization angle of 14.0 deg., indicating that the electrical response contained more than one relaxation process with similar relaxation times. Figure 6 also shows the fitting of the high frequency experimental data which yielded a relaxation frequency of 8.2 x 10^3 Hz. At 40% r.h. the semicircle

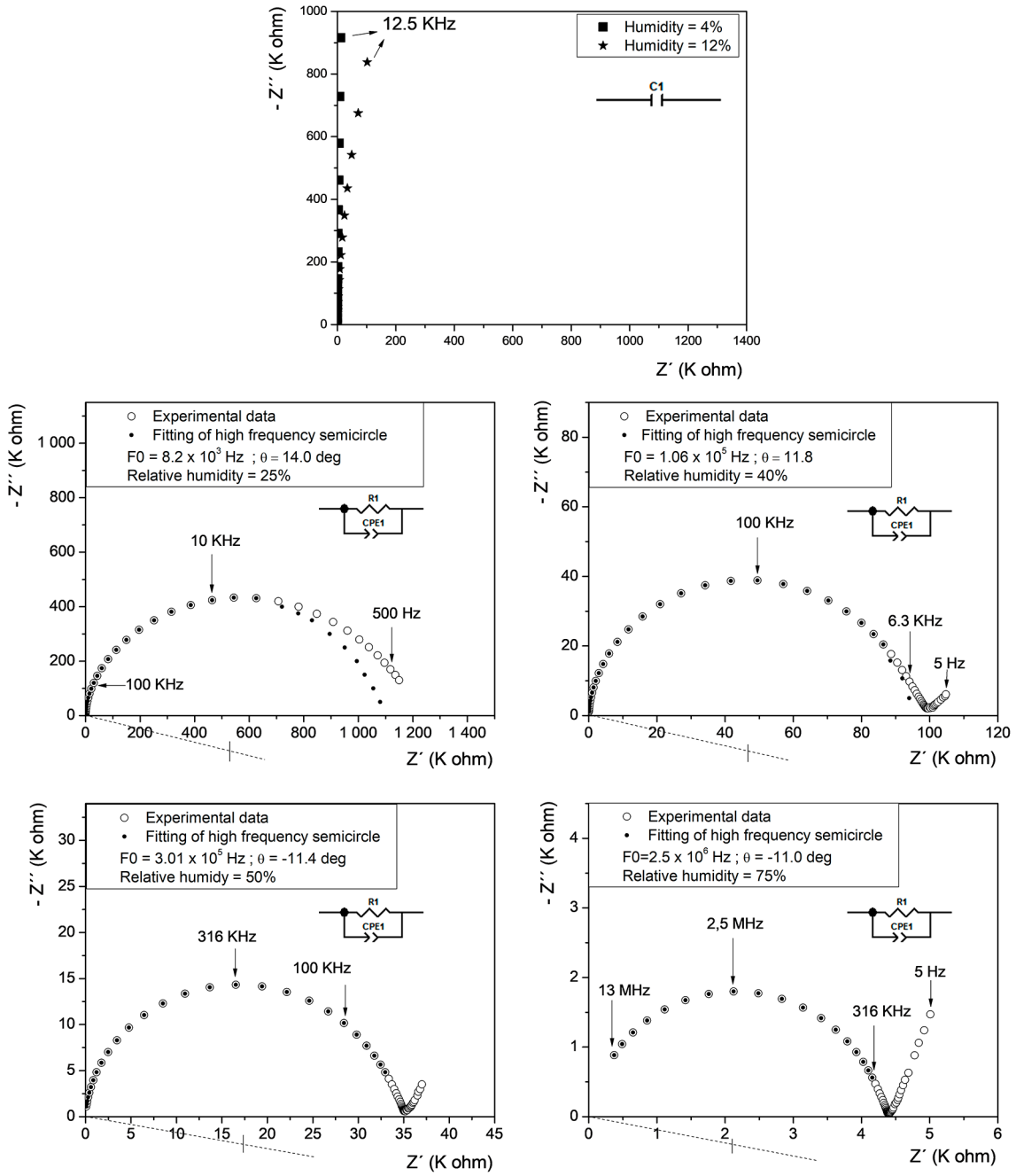

Figure 9. Equivalent circuits and Nyquist plots at room temperature of composition A sintered at 1350ºC with varying relative humidity

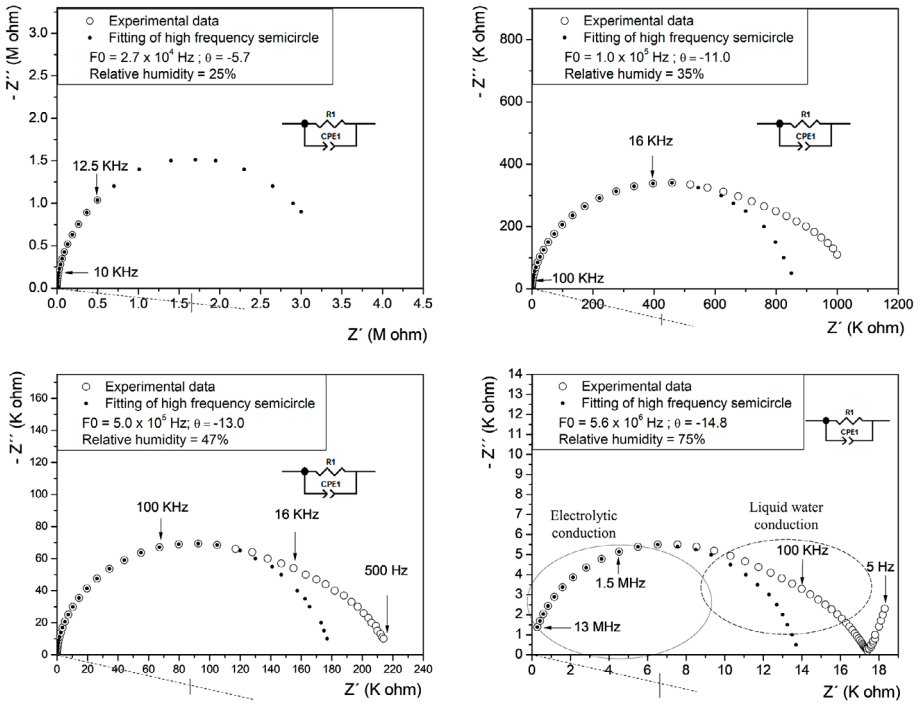

Figure 10. Equivalent circuits and Nyquist plots at room temperature of composition B sintered at 1350ºC with varying relative humidity

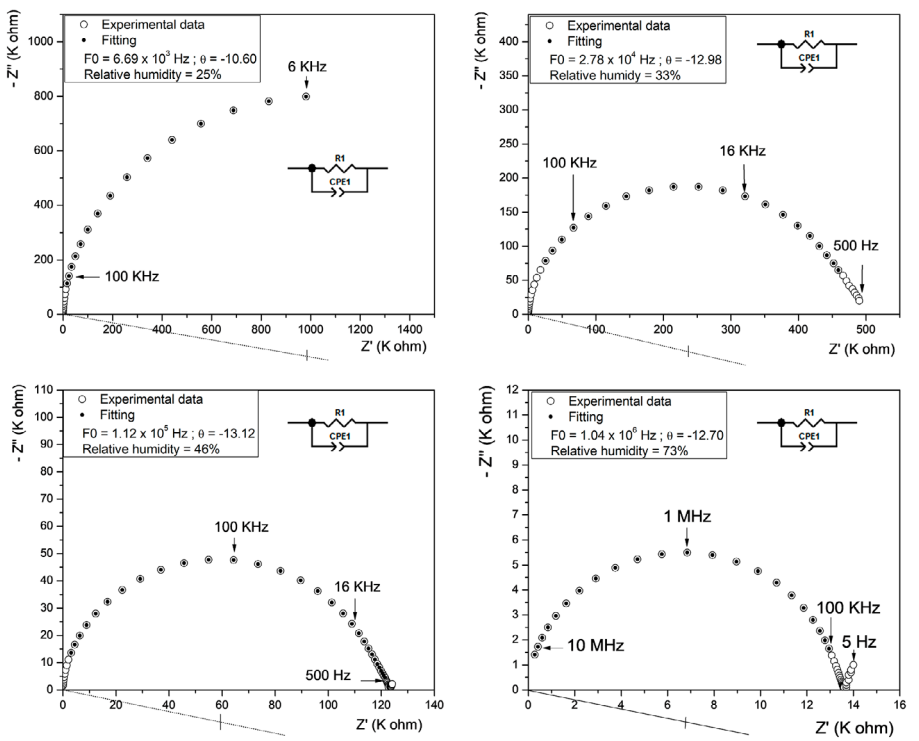

Figure 11. Equivalent circuits and Nyquist plots at room temperature of composition C sintered at 1350ºC with varying relative humidity

showed a lower decentralization angle (11.8 deg) than at 25% r.h., indicating the tendency for a predominant relaxation process which relaxation frequency of 1.06 x 10^5 Hz, obtained by fitting, was in good agreement with that found for distilled water (Figure 6). Hence, the predominant electrical conduction mechanism at 40% r.h. is the same as that of liquid water, i.e., the Grotthuss chain reaction, which may be due either to physically adsorbed water layers or water condensation in pores which critical radius is smaller than that established by the Kelvin equation. It is important to remember that the critical pore radio for $MgAl_2O_4$ is below 300 Å[5] and the Hg intrusion porosimetry technique used in this work is not sensitive for pores lower than this size. Increasing the relative humidity to 50% caused the impedance spectrum to shift to the region of high frequency, indicating the contribution of another electrical conduction mechanism. At 75% r.h. the impedance spectrum showed a semicircle which fitting yielded the relaxation frequency of 2.5 x 10^6 Hz, which was close to that of the electrolytic conduction process (Figure 8), but with significant dispersion indicated by the decentralization angle of 11 deg. Therefore, at 75% r.h. both liquid water and electrolytic conduction mechanisms contributed to the sample's electrical response, but the mechanisms could not be visualized separately because their relaxation times differed by only one order of magnitude. However, the relaxation frequency obtained by fitting (2.5 x 10^6 Hz) was closer to the electrolytic process than liquid water, allowing us to affirm that the predominant mechanism was electrolytic conduction. Electrolytic conduction is caused by ions from the pore surface where water vapor condenses and, according to Kelvin's equation, it is about 10^{-2} μm in this humidity range.

Figure 10 shows the impedance spectra of composition B at various levels of relative humidity and also the fitting of experimental high frequency data. These spectra differed completely from those of composition A in the entire range of relative humidity analyzed. At low relative humidity (25%), only the beginning of a semicircle is visible, i.e., composition B is more resistive than composition A at the same relative humidity. As the relative humidity increased, the spectra became complex, clearly showing the presence of more than one conduction mechanism. While the spectrum of composition A at 40% r.h. was typical of liquid water, in composition B the response of liquid water was visible at 47% r.h., although it was not predominant. This behavior indicates that in composition B there were still numerous pores in which electrical conduction mechanisms typical of low humidity occurred. At high relative humidity (75%), the spectrum exhibited the contribution of liquid water and electrolytic conduction, which were identified as described for composition A. It should be noted that liquid water is not necessarily condensed water. In the spectrum of composition B obtained at 75% r.h., electrolytic conduction occurred in the condensed water. Moreover, the so-called liquid water conduction must have been due to physisorbed water because if it had been condensed water, it would contain ions, and electrolytic conduction would have been predominant, as was the case in composition A.

Figure 11 shows the Nyquist plots for composition C at several levels of relative humidity. The spectra are very simple comparing with compositions A and B. At 33% r.h. processes with low relaxation frequency are predominant, while at 46% r.h. the prevalent mechanism is liquid water conduction. At high r.h. (73%) the predominant mechanism is electrolytic conduction. It is interesting to note that despite the similarity between total open porosity obtained by Hg intrusion porosimetry and grain size for compositions B and C, Figures 3 and 5 respectively, the impedance spectra are appreciably different. This behavior can be attributed to the pore size distribution in the range from 20 to 300 Å, which is not accurately observed through Hg intrusion porosimetry, aspreviously mentioned.

The substitution of Mg^{2+} by Mn^{2+} ions in the $MgAl_2O_4$ structure, as already commented, especially for the MnO content in composition C, is the responsible agent for this special microstructure development, which presents simple impedance spectra, meaning that for each specific humidity range there is a predominant conduction mechanism. Besides simple impedance spectra, composition C showed better response time and reproducibility, as shown in Figures 12 and 13.

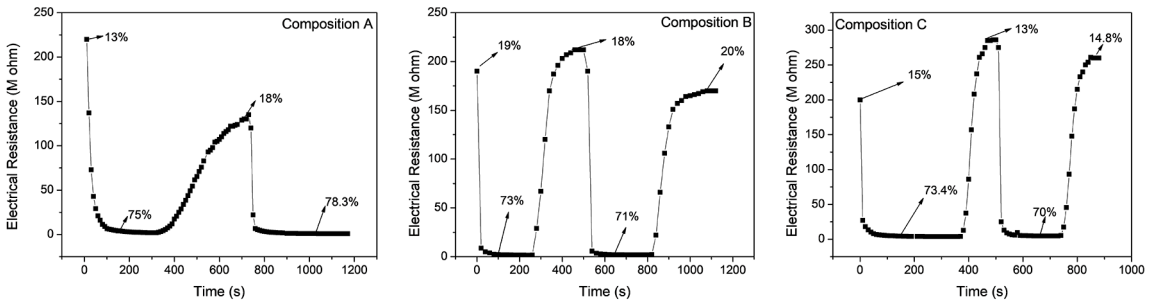

Figure 12. Response time at room temperature of compositions A, B and C sintered at 1350ºC

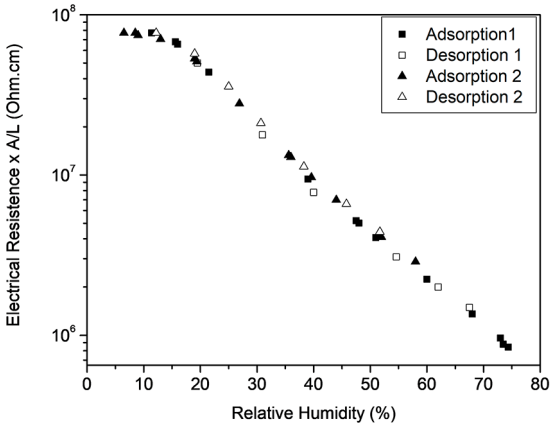

Figure 13. Reproducibility of the electrical resistance of composition C as a function of relative humidity

Therefore, the impedance spectra obtained in this work for samples of $MgAl_2O_4$ with significantly different microstructures allowed to clearly associate electric conduction mechanisms with the relative humidity of the atmosphere in which the sample was submitted. The knowledge acquired in the execution of this work allows us to analyze literature results on impedance spectra as a function of humidity for other materials obtained by different methods.

The literature presents impedance spectra for various other materials as a function of relative humidity. J. Wang et al.[18] analyzed nanometric zirconia film humidity sensors. The spectra are quite simple for relative humidity ranging from 11 to 98%. Based on our analysis here, we can state that electrical conduction mechanisms with low relaxation frequency predominate in nanometric zirconia film even at high relative humidity. The authors showed a Nyquist diagram at 75% r.h. for which the relaxation frequency was about 50 KHz. Although the relaxation frequency for liquid water is 1.17×10^5 Hz, the pore size of nanometric zirconia film was not suitable for water condensation even at 75% r.h. The impedance spectra that P. M. Faia et al.[8] obtained for a TiO_2-WO_3 thin film humidity sensor consisted of a semicircle of high decentralization angles for frequencies below 1 Hz even at high humidity, indicating the absence of a predominant electrical conduction mechanism.

3.3 Response time

The response was analyzed using the four-probe dc technique by subjecting samples to alternately high and low humidity. Composition A showed a very slow response to desorption, as shown in Figure 12. The impedance spectroscopy analysis indicated intense water condensation in this sample due to its single pore distribution, which inhibited water loss during desorption. Composition B showed slower desorption than composition C (Figure 12) because composition B has numerous pores in which water condensation did not occur, as observed by impedance spectroscopy. An electrical response of low relaxation frequency typical of physisorbed water was observed even at high humidity. Composition C showed fast response time due to the same reason that promotes the simple impedance spectra, that is, appropriated microstructure.

Another important characteristic of humidity sensors is reproducibility. Figure 13 shows the behavior of composition C when subjected to several cycles of increasing and decreasing humidity in the range 5 - 75% r.h. The reproducibility was very good, as was expected from the fast response time. Figure 13 also shows that the sample had good sensitivity for humidity levels above 12% r.h.

4. Conclusions

4 mol% of manganese oxide as $MgAl_2O_4$ sintering aid promoted the formation of specific microstructures that yielded relatively simple impedance spectroscopy spectra, making it possible to follow the evolution of the electrical behavior of $MgAl_2O_4$ when exposed to relative humidity in the range of 5 to 80%. The simplicity of the samples impedance spectra, associated with the impedance spectra of distilled water and water containing ions from particles of $MgAl_2O_4$ powder, enabled us to identify the predominant electrical conduction mechanism at each relative humidity.

5. Acknowledgements

The authors are grateful to CNPq for financial support, to CAPES for the scholarships and to LCE for the availability of its facilities.

6. References

1. Traversa E. Ceramic sensors for humidity detection: the state-of-the-art and future developments. *Sensors and Actuators B: Chemical*. 1995;23(2-3):135-156.

2. Chen Z, Lu C. Humidity Sensors: A Review of Materials and Mechanisms. *Sensor Letters*. 2005;3:274-295.

3. Farahani H, Wagiran R, Hamidon MN. Humidity sensors principle, mechanism, and fabrication technologies: a comprehensive review. *Sensors (Basel)*. 2014;14(5):7881-7939.

4. Seiyama T, Yamazoe N, Arai H. Ceramic humidity sensors. *Sensors and Actuators*. 1983;4:85-96.

5. Shimizu Y, Arai H, Seiyama T. Theoretical studies on the impedance-humidity characteristics of ceramic humidity sensors. *Sensors and Actuators*. 1985;7(1):11-22.

6. Gusmano G, Montesperelli G, Nunziante P, Traversa E. Study of the conduction mechanism of $MgAl_2O_4$ at different environmental humidities. *Electrochimica Acta*. 1993;38(17):2617-2621.

7. Faia PM, Furtado CS, Ferreira AJ. AC impedance spectroscopy: a new equivalent circuit for titania thick film humidity sensors. *Sensors and Actuators B: Chemical*. 2005;107(1):353-359.

8. Faia PM, Ferreira AJ, Furtado CS. Establishing and interpreting an electrical circuit representing a TiO_2-WO_3 series of humidity thick film sensors. *Sensors and Actuators B: Chemical*. 2009;140(1):128-133.

9. Hu S, Fu G. Humidity-sensitive properties based on liquid state $LiZnVO_4$-doped SnO_2. *Sensors and Actuators A: Physical*. 2010;163(2):481-485.

10. Doroftei C, Popa PD, Iacomi F. Study of the influence of nickel ions substitutes in barium stannates used as humidity resistive sensors. *Sensors and Actuators A: Physical*. 2012;173(1):24-29.

11. Singh M, Yadav BC. Physics and Technology of Humidity Sensing Through a Solid State Pellet of Cerium Oxide. *Sensors & Transducers*. 2015;186(3):140-147.

12. Chou KS, Lee TK, Liu FJ. Sensing mechanism of a porous ceramic as humidity sensor. *Sensors and Actuators B: Chemical*. 1999;56(1-2):106-111.

13. Gusmano G, Montesperelli G, Traversa E, Mattogno G. Microstructure and Electrical Properties of $MgAl_2O_4$ Thin Films for Humidity Sensing. *Journal of the American Ceramic Society*. 1993;76(3):743-750.

14. Shah J, Kotnala RK, Singh B, Kishan H. Microstructure-dependent humidity sensitivity of porous $MgFe_2O_4$-CeO_2 ceramic. *Sensors and Actuators B: Chemical*. 2007;128(1):306-311.

15. Aoki H, Azuma Y, Asaka T, Higuchi M, Asaga K, Katayama K. Improvement of response characteristics of TiO_2 humidity sensors by simultaneous addition of Li_2O and V_2O_5. *Ceramics International*. 2008;34(4):819-822.

16. Katayama K, Hasegawa H, Noda T, Akiba T, Yanagida H. Effect of alkaline oxide addition on the humidity sensitivitiy of Nb_2O_5-doped TiO_2. *Sensors and Actuators B: Chemical*. 1990;2(2):143-149.

17. Kim TY, Lee DH, Shim YC, Bu JU, Kim ST. Effects of alkaline oxide additives on the microstructure and humidity sensitivity of $MgCr_2O_4$-TiO_2. *Sensors and Actuators B: Chemical*. 1992;9(3):221-225.

18. Wang J, Su MY, Qi JQ, Chang LQ. Sensitivity and complex impedance of nanometer zirconia thick film humidity sensors. *Sensors and Actuators B: Chemical*. 2009;139(2):418-424.

19. Miranda AR, Vannucci A, Pontuschka WM. Impedance spectroscopy of water in comparison with high dilutions of lithium chloride. *Materials Research Innovations*. 2011;15(5):302-309.

20. Izumi K, Miyazaki S, Yoshida S, Mizokawa T, Hanamura E. Optical properties of 3d transition-metal-doped $MgAl_2O_4$ spinels. *Physical Review B*. 2007;76(7):075111.

21. Singh V, Chakradhar RPS, Rao JL, Kim DK. Synthesis, characterization, photoluminescence and EPR investigations of Mn doped $MgAl_2O_4$ phosphors. *Journal of Solid State Chemistry*. 2007;180(7):2067-2074.

22. Shannon RD. Revised effective ionic radii and systematic studies of interatomic distances in halides and chalcogenides. *Acta Crystallographica Section A*. 1976;32:751-767.